Journal of
Nanoscience and Nanotechnology
Vol. 8, 479–492, 2008

First-Principles Study of Silicon Nanocrystals: Structural and Electronic Properties, Absorption, Emission, and Doping

Stefano Ossicini[1,*], O. Bisi[1], Elena Degoli[1], I. Marri[1], Federico Iori[2], Eleonora Luppi[2], Rita Magri[2], Raffaele Poli[2], G. Cantele[3], D. Ninno[3], F. Trani[3], M. Marsili[4], O. Pulci[4], V. Olevano[5], M. Gatti[6], K. Gaal-Nagy[6], A. Incze[6], and G. Onida[6]

[1] *CNR-INFM-S*[3] *and Dipartimento di Scienze e Metodi dell'Ingegneria, Università di Modena e Reggio Emilia, via G. Amendola 2, I-42100 Reggio Emilia, Italy*
[2] *Dipartimento di Fisica, Università di Modena e Reggio Emilia, via Campi 213/A, Modena I-41100, Italy*
[3] *CNR-INFM-Coherentia and Università di Napoli "Federico II," Dipartimento di Scienze Fisiche, Complesso Universitario Monte S. Angelo, Via Cintia, I-80126 Napoli, Italy*
[4] *European Theoretical Spectroscopy Facility (ETSF) and Dipartimento di Fisica - Università di Roma "Tor Vergata," Via della Ricerca Scientifica 1, I-00133 Roma, Italy*
[5] *European Theoretical Spectroscopy Facility (ETSF) and Laboratoire d' Etudes des Propriètès Electroniques des Solides - UPR 11 CNRS - F-38042 Grenoble, France*
[6] *European Theoretical Spectroscopy Facility (ETSF) and Dipartimento di Fisica, Università di Milano, Via Celoria 16, I-20133 Milano, Italy*

Total energy calculations within the Density Functional Theory have been carried out in order to investigate the structural, electronic, and optical properties of un-doped and doped silicon nanostructures of different size and different surface terminations. In particular the effects induced by the creation of an electron-hole pair on the properties of hydrogenated silicon nanoclusters as a function of dimension are discussed in detail showing the strong interplay between the structural and optical properties of the system. The distortion induced on the structure by an electronic excitation of the cluster is analyzed and considered in the evaluation of the Stokes shift between absorption and emission energies. Besides we show how many-body effects crucially modify the absorption and emission spectra of the silicon nanocrystals. Starting from the hydrogenated clusters, different Si/O bonding at the cluster surface have been considered. We found that the presence of a Si—O—Si bridge bond originates significative excitonic luminescence features in the near-visible range. Concerning the doping, we consider B and P single- and co-doped Si nanoclusters. The neutral impurities formation energies are calculated and their dependence on the impurity position within the nanocrystal is discussed. In the case of co-doping the formation energy is strongly reduced, favoring this process with respect to the single doping. Moreover the band gap and the optical threshold are clearly red-shifted with respect to that of the pure crystals showing the possibility of an impurity based engineering of the absorption and luminescence properties of Si nanocrystals.

Keywords: Silicon Nanocrystals, Band Structure, Calculations, Optical Properties, Emission Mechanism, Doping.

1. INTRODUCTION

The complete comprehension and the control of the properties of materials is crucial for improving the information technology on which our modern life is built. The ever increasing demands from distributed information systems are stimulating the research and the technology development. Theory has a central role because a microscopic understanding represents a fundamental step towards the innovation, design, and fabrication of new materials and devices. The ability to describe structural, electronic, and optical properties of new materials with accurate first-principles methods is hence of fundamental importance.

*Author to whom correspondence should be addressed.

In particular silicon microelectronics devices have revolutionized our life in the second half of the last century. Integration and economy of scale are the two key ingredients for the silicon technological success. Silicon has a band gap of 1.12 eV that is ideal for room temperature operations and has an oxide that allows the processing flexibility to place today more than 10^8 transistors on a single chip. The extreme integration levels reached by Si microelectronics industry have permitted high speed performance and unprecedented interconnection levels. The present interconnection degree is sufficient to cause interconnect propagations delays, overheating, and information latency between single devices. To overcome this bottleneck, photonic materials, in which light can be generated, guided, modulated, amplified, and detected, need to be integrated with standard electronics circuits to combine the information processing capabilities of electronic data transfer and the speed of light. In particular, chip to chip or even intra-chip optical communications all require the development of efficient optical functions and their integration with state-of-art electronic functions.[1]

Silicon is the desired material, because Si-based optoelectronics would open the door to faster data transfer and higher integration densities at low cost. Si microphotonics has boomed during these last years. Almost all the various photonic devices have been demonstrated,[1,2] the main limitation of silicon photonics remains the lack of any practical Si-based light source.

Several attempts have been employed to engineer luminescent transitions in an otherwise indirect material.[1] After the initial impulse given by the pioneering work of Canham on photoluminescence (PL) from porous silicon (PS),[3] nanostructured silicon has received extensive attention (for review see Refs. [4–15]). This activity is mainly centered on the possibility of getting relevant optoelectronic properties from nanocrystalline Si. It is generally accepted that the quantum confinement, caused by the restricted (nanometric) size, is essential for the visible light emission in Si nanostructures, but some controversial interpretations of the PL properties of Si nanocrystals (Si-nc) still exist.[1,10]

The theoretical investigation of phenomena such as the Stokes shift (difference between absorption and emission energies), the PL emission energy versus nanocrystal size, etc. can give a fundamental contribution to the understanding of how the optical response of such systems can be tuned. An interesting amount of work has been done regarding excited Si-nc,[4–15] but a clear comprehension of some aspects is still lacking. The question of surface effects, in particular oxidation, has been addressed in the last years. Both theoretical calculations and experimental observations have been applied to investigate the possible active role of the interface on the optoelectronic properties of Si-nc. Different models have been proposed: Baierle et al.[16] have considered the role of the surface geometry distortion of small hydrogenated Si clusters in the excited state. Wolkin et al.[17] have observed that oxidation introduces defects in the Si-nc band-gap which pin the transition energy. They claimed the formation of a Si=O double bond as the pinning state. The same conclusion has been recently reached by other authors,[18–21] whereas Vasiliev et al.[22] have pointed out that similar results can be obtained also for O connecting two Si atoms (single bond) at the Si-nc surface. The optical gain observed in Si-nc embedded in SiO_2 formed by different techniques[23–26] has given a further impulse to these studies. Interface radiative states have been suggested to play a key role in the mechanism of population inversion at the origin of the gain.[23,24,27] Nevertheless many researchers are still convinced of the pure quantum confinement model and they are focusing the efforts mainly on the self-trapped excitonic effects[28,29] in order to explain the differences between their results and the experimental outcomes.

Other possibilities to circumvent the indirect gap behavior of bulk Si are given by the introduction in the Si-nc of an isoelectronic impurity[1,10] or by simultaneous *n*- and *p*-type impurity doping.[30] In a series of intriguing papers Fujii and collaborators[30–32] have demonstrated the possibility to control the PL properties of Si-nc by simultaneous doping with B and P impurities. They have shown not only that the PL intensity of co-doped Si-nc is always higher than that of either P- or B doped Si-nc, but also that it is even higher than that of the un-doped Si-nc. Besides, under resonant excitation condition, the co-doped samples did not exhibit structures related to momentum-conserving phonons, suggesting that in this case the quasidirect optical transitions are predominant.

In this paper we present a comprehensive first-principles study of the structural, electronic, and optical properties of un-doped and B and P single and simultaneously doped Si-nc. Since in all cases the quasidirect optical transitions are the most relevant, the phonon-assisted ones are not included in the optical calculations. The aim is to investigate in a systematic way their structural, electronic, and stability properties as a function of size as well as pointing out the main changes induced by the nanocrystal excitation. A comparison between the results obtained using different Density Functional Theory (DFT)-based methods will be presented. The absorption and emission spectra and the effects induced by the creation of an electron-hole pair are also calculated and discussed in detail including many-body effects for both hydrogenated and oxidized Si-nc.

In Section 2 we focus on the structural properties, calculated for H-terminated Si-nanocrystals both in the ground- and in an excited-state configuration, corresponding to the first allowed optical transition, showing how a different electronic configuration can modify such structural properties and give rise to the Stokes shift between absorption and emission energies.

In Section 3 we present the results concerning the role of different Si/O bond geometries at the cluster's surface

on the electronic properties of the Si-nc. Moreover we present here both absorption and emission spectra fully including excitonic effects.

In both Sections 2 and 3 a comparison between different ab-initio DFT-based methods is performed and discussed.

In Section 4 the effects of boron and phosphorus single and co-doping on the impurity formation energies and on the electronic and optical properties of Si-nc are calculated and discussed in details.

Finally, some conclusions are presented in Section 5.

2. STRUCTURAL AND ELECTRONIC PROPERTIES OF SI-NANOCRYSTALS: GROUND STATE VERSUS EXCITED STATE

The study of the Si-nc has been done within the DFT, using a pseudopotential, plane-wave approach.[33] All the calculations related to this section have been performed with the ABINIT code.[34] Norm-conserving, non-local Hamann-type pseudopotentials have been used. The Kohn-Sham wave functions have been expanded within a plane-wave basis set, choosing an energy cutoff of 32 Ry. Each Si-nc has been embedded within a large cubic supercell, containing sufficient vacuum in order to have nanocrystal interactions negligible. Convergence with respect to both energy cutoff and supercell side has been checked. Gradient-corrected Perdew-Burke-Ernzerhof (GGA-PBE) exchange-correlation functional has been used for both structural and electronic properties calculations.

The calculations for each cluster have been performed both in the ground and the excited state where the excited state is approximated with the electronic configuration in which the highest occupied single-particle state (HOMO) contains a hole (h), while the lowest unoccupied single-particle state (LUMO) contains the corresponding electron (e). The structural properties have been determined by allowing full relaxation of each Si-nc until the maximum force was lower than 5×10^{-5} Ha/Bohr. The starting atomic structures for all clusters has been fixed with all Si atoms occupying the same position as in the bulk crystal, and passivating the surface with H atoms placed along the bulk crystal directions, at a distance determined by studying the SiH_4 molecule. Excitation of nanoclusters has been studied calculating pair-excitation energies[36–38] taking into account the formation of an electron-hole pair (constrained DFT method (CDFT) which has been proven to work well for zero-dimensional systems). A schematic representation is drawn in Figure 1. The nanocluster excitation (from configuration (1) to (2) in Fig. 1) occurs with the atomic positions fixed in their ground-state configuration. We define, following Ref. [37], $E(N)$ the N-electron ground-state energy and $E(N, e-h)$ the total energy of the nanocluster calculated with the electron-hole pair constraint. The difference $\varepsilon_{\rm ex}^{\rm A} = E(N, e-h) - E(N)$ gives the

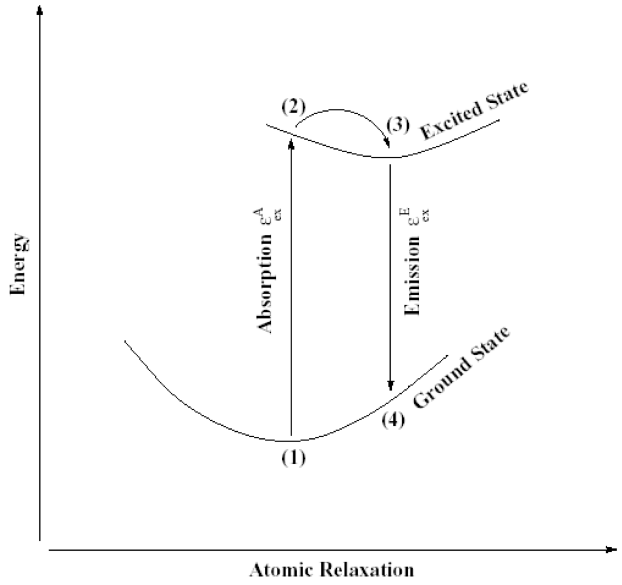

Fig. 1. Schematic representation of a Stokes shift relaxation. In configuration (1), the cluster is in its electronic ground state, and the atomic geometry is relaxed to its lower energy configuration. On absorption of a photon, the nanocluster undergoes a vertical electronic excitation from configuration (1) to configuration (2). Once in the excited electronic state, the atomic geometry of the cluster relaxes to a lower energy configuration (from configuration (2) to configuration (3)). Finally, the excited electron and hole recombine via another vertical transition, configuration (3) to configuration (4). The Stokes shift is defined as $\varepsilon_{\rm ex}^{A} - \varepsilon_{\rm ex}^{E}$.

energy needed for the creation of the pair, and defines the absorption edge (let us note that, with reference to Fig. 1, $E(N) \equiv E_1$ and $E(N, e-h) \equiv E_2$, E_1 and E_2 being the cluster total energies in the configuration 1 and 2 respectively). It should be noted that the quasi-particle gap defined as $E(N+1) + E(N-1) - 2E(N)$, and calculated from the $N+1$-, $N-1$-, and N-electron total energies, neglects the effect of the Coulomb attraction between the electron and the hole.

After excitation, due to the change in the charge density, relaxation occurs until the atoms reach a new minimum energy configuration, in presence of the electron-hole pair (from configuration (2) to (3) in Fig. 1). This modifies the electronic spectrum, implying that the levels involved in the emission process (electron-hole recombination, from configuration (3) to (4) in Fig. 1) change. The emission energy can be defined as $\varepsilon_{\rm ex}^{\rm E} = E'(N, e-h) - E'(N)$, where $E'(N, e-h)$ and $E'(N)$ are the nanocluster total energies evaluated in presence and in absence of the electron-hole pair respectively, with the atoms occupying the equilibrium positions of the excited state (see configurations (3) and (4) in Fig. 1, with $E'(N, e-h) \equiv E_3$, $E'(N) \equiv E_4$). The difference $\Delta E^{\rm Stokes} = (\varepsilon_{\rm ex}^{A} - \varepsilon_{\rm ex}^{E})$ (which, in Fig. 1, corresponds to $(E_2 - E_1) - (E_3 - E_4)$) defines the Stokes shift. Therefore, a contribution to the Stokes shift arises from relaxation after excitation of the nanocluster. This model assumes that the relaxation under excitation is faster than the electron-hole recombination. The

calculations performed are not spin-polarized, however it should be noted that similar computations have been done by Franceschetti and Pantelides[35] within local spin-density approximation, showing that the singlet–triplet splitting is significantly smaller than the Stokes shift.

The structural properties of semiconductor nanoclusters have been calculated performing for each cluster the geometry relaxation both in the ground- and excited-state configuration and without any symmetry constraint. To qualitatively appreciate the structural changes, we have plotted in Figure 2 the relaxed structures of some clusters, both in their ground- and excited-state configurations. The Si—H bond lengths remain practically unchanged for both the ground and excited state configurations, in contrast with the Si—Si distances (indicating that the excitation concerns the Si shells rather than being simply localized on the surface). The first-, second-, third-, and fourth-neighbor distances are almost unchanged, with respect to bulk values, in the ground-state configuration, while significative deviations are induced by the excitation. Therefore, the presence of an electron-hole pair in the clusters causes a strong deformation of the structures with respect to their ground-state configuration, and this is more evident in small systems. This is what we expect, since for large clusters the charge density perturbation is distributed throughout all the structure, and the distortion effect being local becomes less evident (only small adjustments of bonds and angles occur with respect to the ground state). On reducing the dimension, such effect can induce large distortions of the structure, which for Si_1H_4 and Si_5H_{12} are particularly strong (see Fig. 2). Similar results have been found in Ref. [39], which points out a contraction effect on the average bond lengths, approaching the bulk value for H—Si-nc with diameter of about 20 Å as well as the absence of a uniform behavior for the excited structures.[40]

The structural modifications are immediately reflected into the electronic structure. In Figure 3 we show the HOMO-LUMO gap for both the ground and excited states together with the absorption and emission energies calculated as previously described (see Fig. 1). Let us recall that we calculate the absorption gap with the atoms fixed at the ground-state relaxed positions as the difference between the total energy of the cluster in presence of the electron-hole pair and the total energy in the ground-state configuration. The emission gap is calculated in a similar way, but with the relaxed geometry of the excited state. The absorption by the cluster in its ground state configuration induces a transition between the HOMO and LUMO levels, which

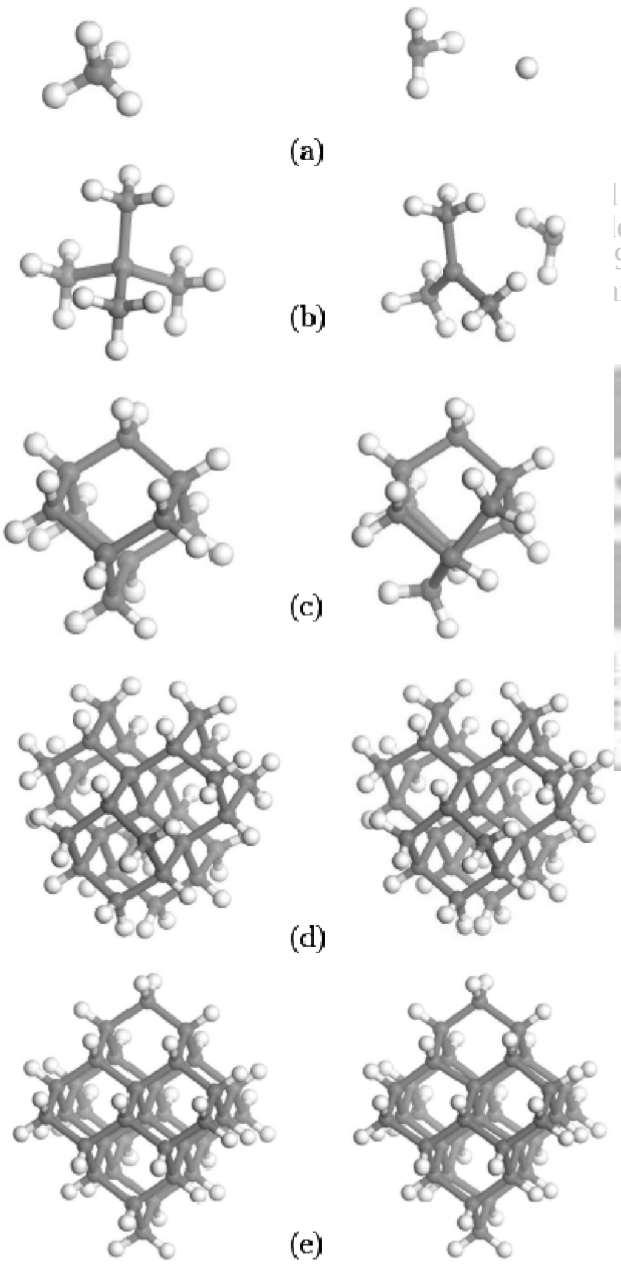

Fig. 2. Calculated structures for the (a) Si_1H_4, (b) Si_5H_{12}, (c) $Si_{10}H_{16}$, (d) $Si_{29}H_{36}$, and (e) $Si_{35}H_{36}$ clusters at relaxed geometry in the ground- (left panels) and excited-state (right panels) configuration.

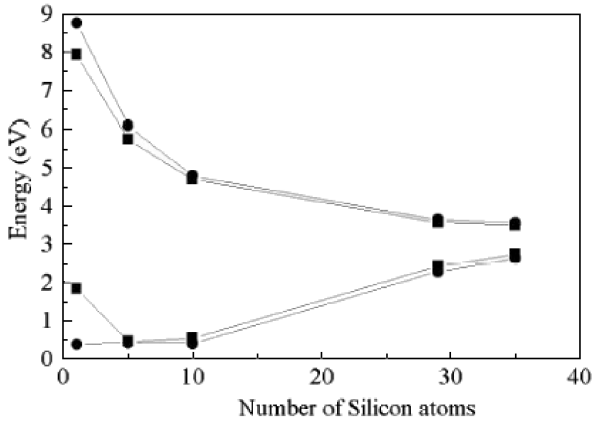

Fig. 3. Absorption (upper curves) and emission (lower curves) values calculated from both pair-excitation energies (circles) and HOMO-LUMO gaps (squares) for the Si_1H_4, Si_5H_{12}, $Si_{10}H_{16}$, $Si_{29}H_{36}$, and $Si_{35}H_{36}$ clusters. The lines are guides for the eyes.

Table I. Stokes shift values for hydrogenated Si clusters: Present work versus theoretical data present in literature.

		Theory					
H—Si clusters	Diameter (nm)	This work	Ref. [38]		Ref. [35]	Ref. [46]	Ref. [47]
Si_1H_4	0.0	8.38					
Si_5H_{12}	0.45	5.67					
$Si_{10}H_{16}$	0.55	4.40	LDA	QMC			
$Si_{29}H_{36}$	0.9	1.35	0.69	1.0	2.92	0.22	0.70
$Si_{35}H_{36}$	1.1	0.92	0.57	0.8			1.67
$Si_{66}H_{64}$	1.3		0.50				
$Si_{87}H_{76}$	1.5		0.22		0.32		
$Si_{29}H_{24}$	0.8	0.84	0.34	0.4			1.17

for all these clusters is optically allowed (nonzero dipole matrix element). Such a transition is followed by a cluster relaxation in the excited state configuration giving rise to distorted geometries (as shown in Fig. 2) and to new LUMO and HOMO, whose energy difference is smaller than that in the ground-state geometry. It is between these two last states that emission occurs and it is worth pointing out how such a shift changes as a function of the dimension.

A great number of papers present in the literature (for a recent review see Ref. [10]) consider the HOMO-LUMO gaps of the ground and excited state as the proper absorption and emission energies; this approximation is worse the smaller is the cluster. In fact, from Figure 3 it is clearly seen that the difference between absorption and HOMO-LUMO ground state (GS) gap and between emission and HOMO-LUMO excited state (EXC) gap is the larger the smaller is the H—Si-nc (Delerue et al.[41] have pointed out that for clusters with diameter larger than 1.2 nm there is a cancellation between self-energy correction and Coulomb term: thus the lowest excitonic energy is "correctly" predicted by the single-particle band gap. We note from Figure 3 that, in our calculations, on going from smaller to larger clusters the difference between the HOMO-LUMO gap in the ground state and the absorption gap becomes smaller). In particular the GS HOMO-LUMO gap tends to be smaller than the absorption energy while the EXC HOMO-LUMO gap tends to be larger than the emission energy. In conclusion, trying to deduce the Stokes shift simply from the HOMO-LUMO gaps leads to errors especially for small clusters.

When comparing our results for the ground state with other DFT calculations we note that there is in general a good agreement. Actually regarding Si_1H_4 Grossman et al.[42] have found 7.8 eV for the HOMO-LUMO gap while Onida and Andreoni[43] have obtained 8.1 eV; these values have to be compared with our calculated 7.93 eV result. Our 3.65 eV calculated absorption gap for $Si_{29}H_{36}$ is in nice agreement with the 3.6 eV[44] obtained with the same method both by Puzder et al.[38] and Franceschetti et al.[35] It is worth mentioning that our results for the absorption gaps of the Si_1H_4 (8.76 eV) and Si_5H_{12} (6.09 eV) clusters agree quite well with the experimental results of Itoh et al.[45] Using synchrotron radiation in the gaseous phase they have found excitation energies of 8.8 eV and 6.5 eV respectively.

Regarding the Stokes shift, really few data exist in literature as Table I shows,[35, 38.46, 47] and, in particular for really small H—Si-nc (from Si_1H_4 to $Si_{10}H_{16}$), no data exist. Our results show a dependence of the Stokes shift from the H—Si-nc size in accordance with Puzder et al.[38] and Franceschetti et al.[35] although our outcomes stay in the middle with respect to them. The discrepancies could be due to the different codes used: a DFT-GGA-PBE non-spin-polarised calculation in our case, a DFT-LDA (Local Density Approximation) singlet–triplet calculation in the case of Puzder where the total energies of the excited states have been computed assuming a triplet spin configuration, a DFT-LSDA (Local Spin Density Approximation) with ultrasoft pseudopotentials for Franceschetti. Experimentally, very few measurements exist on hydrogenated Si clusters and what emerges is a decreasing of the Stokes shift value with increasing clusters dimension.[48, 49]

A last point must be stressed here. Recent results concerning optical gain in silicon nanoclusters embedded in a SiO_2 matrix have been explained within a four-level, rate equation model.[23, 24, 27] In that case the electronic spectrum becomes more complex due to the presence of oxygen that can induce localized states within the nanocrystals gap (see Section 3). Anyway, the presence of the Stokes shift as depicted above can still give a possible interpretation of the nature of the levels invoked by the model. They can be identified with the HOMO and LUMO states in the ground- and excited-state configuration. Starting from a silicon nanocluster in its ground state, the pumping mechanism induces the HOMO-LUMO transition followed by a structural relaxation which leads to a more favorable geometrical arrangement of the atoms. This modifies the band edges, giving rise to new, differently localized HOMO and LUMO states now involved in the emission process.

Concerning the optical properties of the hydrogenated clusters and the comparison between different ab-initio methods, Figure 4 shows the absorption spectra of the Si_5H_{12} cluster calculated using different DFT-based methods.[34] In particular we have performed a LDA calculation in the Random Phase Approximation

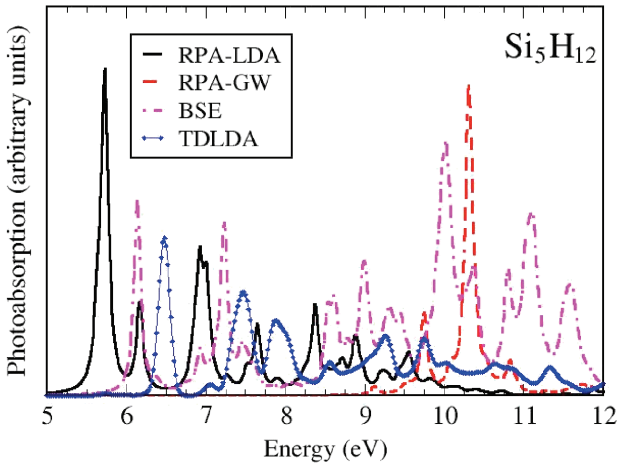

Fig. 4. Absorption spectra of the Si_5H_{12} cluster calculated using different DFT based methods: LDA-RPA black (black), GW-RPA red (dark gray), BSE violet (light gray), TDLDA blue (light black). BSE and TDLDA calculations naturally include local fields effects (LF). In the case of TDLDA, the correlation contribution to the kernel gives small corrections to the "LF only" result.

(RPA-LDA, neglecting Local Fields), we have calculated the self-energy corrections within the GW method (RPA-GW), then the excitonic effects have been included both performing a time dependent local density approximation (TDLDA) calculation and a fully excitonic calculation through the Bethe-Salpeter equation (BSE). As usual we note an underestimation of the optical gap in the RPA-LDA scheme with respect to the experimental value (6.5 eV).[45] Concerning the RPA-GW method (the self-energy corrections) the main result is a huge opening of the optical gap. The effects of the electron-hole interaction on the optical properties (BSE result) is also quite large, the excitonic binding energy is of the order of 3 eV, resulting in a sort of compensation with respect to the GW opening. Interestingly the BSE and TDLDA results are similar regarding the absorption onset and in agreement with the experimental result.

3. ABSORPTION AND EMISSION SPECTRA: MANY BODY EFFECTS AND OXYGEN ROLE

The aim of the present section is to investigate the mechanisms involved in the modification of the electronic and optical properties of Si nanocrystals when they are oxidized. We have studied six different clusters. Computational details are the same as in the previous section, except that LDA instead of GGA has been used.[50] We have simulated the oxidation considering the adamantane-like $Si_{10}H_{16}$ nanocrystal (left of the first row in Fig. 5), and by adding an oxygen atom to its ground state structure. This can be made either without removing H atoms (hence leading to $Si_{10}H_{16}O$, shown on the right of the first row

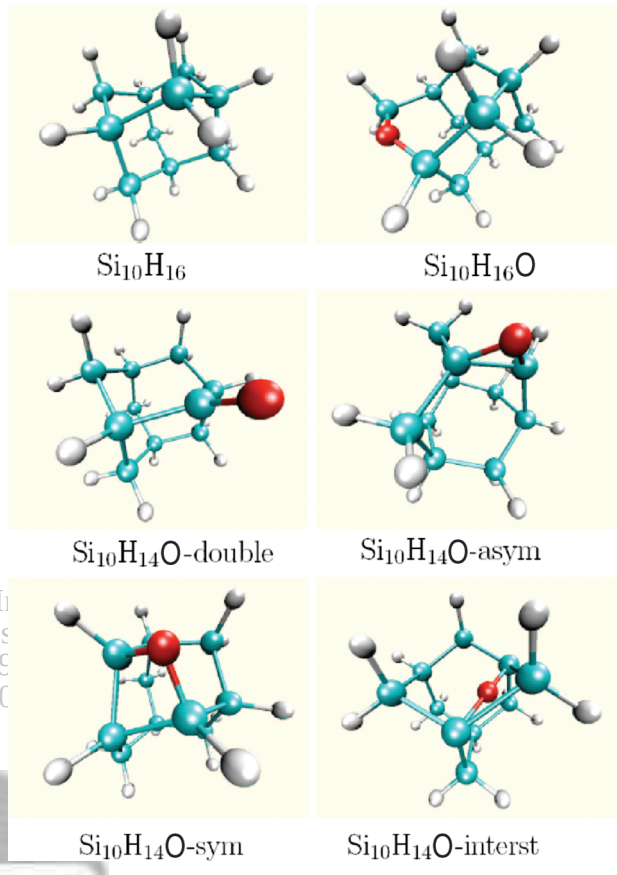

Fig. 5. Structure of $Si_{10}H_{16}$, $Si_{10}H_{16}O$, and the four isomers of $Si_{10}H_{14}O$. In the ball and stick representation, Si is light blue (gray), H is gray (light gray), and O is red (dark gray). All clusters have very reduced symmetry, except for the unoxidized $Si_{10}H_{16}$, which has the full T_d symmetry.

of Fig. 5, with an O atom placed on one of the 12 equivalent Si—Si bonds of $Si_{10}H_{16}$), or by replacing a pair of hydrogens with one oxygen (in this case, no Si—Si bond is broken). In the latter case, one is lead to one of the four different isomers of $Si_{10}H_{14}O$, shown on the two bottom rows of Figure 5. In all the isomers, oxygen is covalently bonded to silicon, with either a double bond ("double" isomer, left of the third row, containing a Si=O bond like in the silanone H_2SiO structure), or with different kinds of bridge (i.e., Si—O—Si bonds). In particular, oxygen can make a bridge between two "first neighbors" or "second neighbors" Si atoms ("asym" and "sym" isomers, shown, respectively, on the right of the second row and on the left of the bottom row), or it can lay in an "interstitial" position inside the Si_{10} cage ("interst" isomer, bottom-right of the figure).

Firstly we have considered the structural modifications induced by oxidation of $Si_{10}H_{16}$.[50] As expected, Si—H bond lengths are almost unaffected; however, also the Si—Si bonds are found to undergo very limited changes. Bond angles, on the contrary, register very large changes, up to 37% in $Si_{10}H_{14}O$-sym. The isomer with

double Si=O bond (i.e., $Si_{10}H_{14}O$-double) undergoes smaller relaxations than isomers with bridge bonds: this observation is in agreement with the results of Luppi and Ossicini for other nanocrystals.[19] Moreover, in accordance with the works of Puzder et al.[38] we find that $Si_{10}H_{14}O$-sym (the stablest isomer) has a larger binding energy (by 1.7 eV) than $Si_{10}H_{14}O$-double. The relative stability of the other bridge-bonded isomer ($Si_{10}H_{14}O$-asym) is very similar to that of the double-bonded cluster (i.e., +1.6 eV), while the interstitially-bonded isomer ($Si_{10}H_{14}O$-interst) is found at a significantly higher energy (+2.6 eV) with respect to $Si_{10}H_{14}O$-sym. In $Si_{10}H_{14}O$-double the Si=O bond has a very similar length (1.529 Å) as the one obtained by Luppi and Ossicini $Si_{14}H_{18}O$ (1.524 Å); the strain of Si—Si bond lengths and the angle variation due to oxidation are also essentially the same. The structural modification induced by the creation of a Si—O—Si bridge over a covalent Si—Si bond can be compared with those taking place on Si surfaces exposed to oxygen.

Besides structural modifications, oxidation induces significant changes in the electronic properties. First, one expects a splitting of the degenerate Kohn-Sham levels of $Si_{10}H_{16}$, due to the symmetry reduction; second, adding an oxygen atom will introduce electronic states with respect to the nonoxidized cluster. Furthermore, there are oxygen-related states appearing inside the energy region of the $Si_{10}H_{16}$ HOMO-LUMO gap. As it has been already described in previous works[19, 22, 38, 51] oxidation of the considered system induces hence a reduction of the HOMO-LUMO gap. Our results for the different systems studied are summarized in Table II. An important remark which comes out from the analysis of our results is that the intensity of the gap reduction depends more strongly on the specific isomer considered than on the type of bond. In agreement with Puzder et al.[38] and Luppi and Ossicini[19] we find that the formation of a double bond determines a strong reduction of the gap; in comparison, the gap reduction in $Si_{10}H_{14}O$-sym is small. However, in the remaining two isomers with bridge bond the calculated gap turns out to be even smaller than in $Si_{10}H_{14}O$-double.

To date very few papers have addressed the issue of the excited-state configurations, which is mostly relevant for small clusters with a high surface to volume ratio. Theoretically their description has been performed using the so called CDFT method,[33, 35, 38, 52] the method that has been outlined and used in the previous Section 2 (see Fig. 1). In this section we calculate not only the transition energies but also the absorption and emission optical spectra. For both the ground (configuration (1) in Fig. 1) and excited state relaxed geometry (configuration (3) in Fig. 1), the transition energies and the optical response Im $\varepsilon_{NC}(\omega)$ (the imaginary part of the nanocrystal dielectric function) are evaluated through first-principle calculations[53] also beyond the one-particle approach.

For the absorption and emission spectra we consider the self-energy corrections[54] by means of the GW method and the excitonic effects through the solution of the Bethe-Salpeter equation.[55] The effect of local fields is also included, to take into account the inhomogeneity of the systems. In order to perform emission spectra calculations, we use the excited state geometry and the ground state electronic configuration (configuration (4) in Fig. 1). Thus, strictly speaking, Im $\varepsilon_{NC}(\omega)$ corresponds to an absorption spectrum in a new atomic geometry. In other words, we consider the emission, in first approximation, simply as the time reversal of the absorption.[56] For the first time, the electron-hole interaction is here considered in the emission geometry.

Starting from the $Si_{10}H_{16}$ structure configuration for all clusters, we consider two types of Si/O bonds at its surface: the silanone-like Si=O bond ($Si_{10}H_{14}$=O) and the Si—O—Si bridge bond, where the O atom makes a bridge between two "second neighbors" Si atoms as in the SiO_2 ($Si_{10}H_{14}O$-sym, from here referred as $Si_{10}H_{14}$>O, the stablest isomer). In Figure 6 the Stokes-Shifts (the difference between the absorption and emission gap) calculated with TDLDA (calculations performed using the ABINIT code), GW-BSE (using a 30 Ry cutoff and a number of plane waves up to 8873) and constrained-LDA are shown for the

Table II. HOMO-LUMO gap (in eV), calculated within DFT-LDA for all the oxidized nanocrystals considered. In columns 3–5, the difference Δ with respect to the "clean" $Si_{10}H_{16}$ nanocrystal is reported. Data from Refs. [19, 38] have been estimated from graphical representations.

Cluster	HOMO-LUMO gap This work	Δ This work	Δ Ref. [38]	Δ Ref. [19]
$Si_{10}H_{14}O$-double	2.47	−2.12	−2.1	−2.1
$Si_{10}H_{14}O$-asym	2.42	−2.17		
$Si_{10}H_{14}O$-sym	3.74	−0.85		−0.9
$Si_{10}H_{14}O$-interst	1.95	−2.64		
$Si_{10}H_{16}O$	4.00	−0.59		

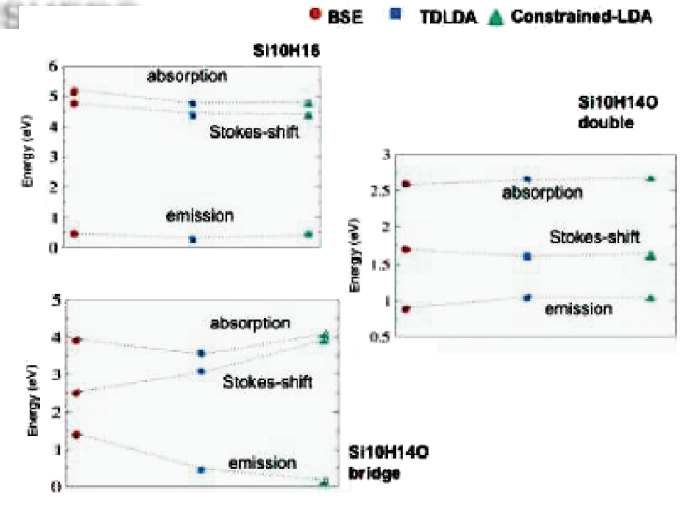

Fig. 6. Calculated Stokes shift for the $Si_{10}H_{16}$, $Si_{10}H_{14}$>O and $Si_{10}H_{14}$=O double clusters. The calculation have been performed using GW+BSE: left, red (dots), TDLDA: middle, blue (squares), constrained LDA: right, purple (triangles) methods.

systems studied. For the hydrogenated system and for the cluster with the double bond the three techniques are in quite good agreement while for the system with the bridge bond there are differences in particular in the emission energy. In this last case the BSE approach shows that more than one *e–h* pair has a substantial contribution to the lower energy exciton. Obviously CDFT works best when the excited state is a linear combination of *e–h* pairs with only one single dominant component. However we notice that, by performing a CDFT calculation, one allows all the orbitals to relax hence the resulting excited state, even if represented by one electron-hole pair, is not the same as the unrelaxed state which enter the linear combination of *e–h* pairs building up the excited state in the BSE scheme. Thus some orbital mixing is present at the CDFT level.

Figure 7 presents the relaxed structures of the considered clusters in their ground state (configuration (1) in Fig. 1) and in the electronic excited state configuration (configuration (3) in Fig. 1). The ionic relaxation has produced structural changes with respect to the initial geometry which strongly depend on the type of surface termination. In $Si_{10}H_{16}$, no much distortion occurs at the surface in the excited state as compared to the ground state geometry, only the Si—Si distances in the core shells are somehow concerned by the excitation. In the case of $Si_{10}H_{14}$=O, the changes are mainly localized near the O atom, in particular the angle between the double bonded O and its linked Si atom is modified (see Fig. 7). In the bridge structure ($Si_{10}H_{14}$>O), instead, the deformation is localized around the Si—O—Si bond determining a considerable strain in the Si—Si dimer distances. These structural changes are reflected in the electronic and optical properties. This is shown in Figure 8, where the calculated absorption and emission spectra are depicted.

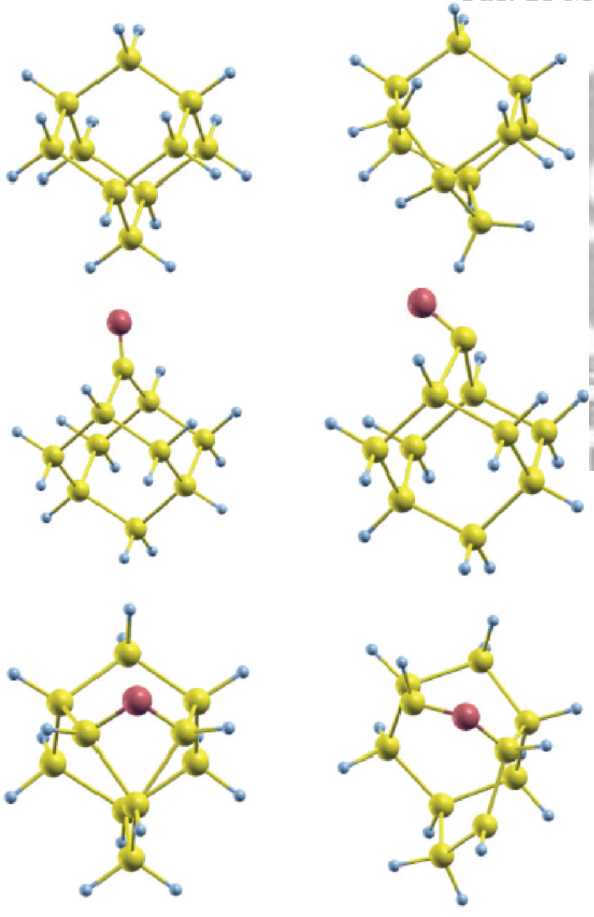

Fig. 7. Calculated structures for the $Si_{10}H_{16}$ (top panel), $Si_{10}H_{14}$=O (central panel) and $Si_{10}H_{14}$>O (bottom panel) clusters at relaxed geometry in both the ground- (left panels) and excited-state (right panels). The Si atoms are yellow (gray), the H atoms are light blue (light gray), and the O atom is red (black).

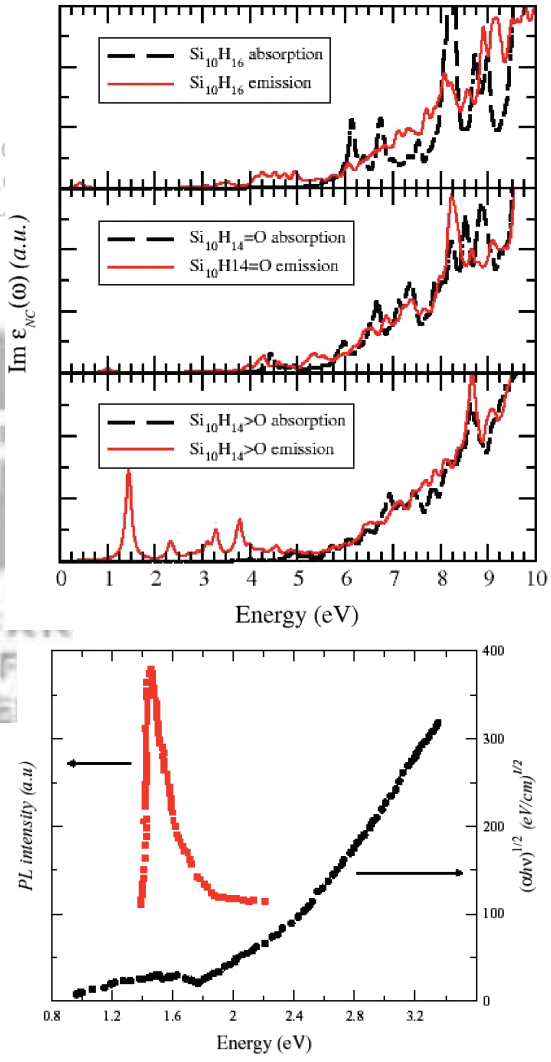

Fig. 8. Up: Imaginary part of the dielectric function (in arbitrary units) for the three Si-nc describing Absorption (dashed line, black) and Emission (solid line, red) spectra in the ground state and excited state geometries, respectively. $Si_{10}H_{16}$ (top panel), $Si_{10}H_{14}$=O (central panel), and $Si_{10}H_{14}$>O (bottom panel). In the calculation self-energy (GW), local-field and excitonic effects (BSE-LF) are fully taken into account. In all cases we have used the same unit cell, thus the intensities of the spectra are comparable. Down: experimental results (red: emission and black: absorption by Ma et al.[57]).

In the figures, each panel reports the imaginary part of the dielectric function for absorption (dashed line) and emission (solid line) of the three considered clusters, the hydrogenated and the two oxidized ones. Self-energy, local-field, and excitonic effects (BSE-LF) are fully taken into account.

Concerning the absorption spectra (Fig. 8, dashed lines), all three cases show a similar smooth increase in the absorption features. The situation for the emission-related spectra is clearly different (Fig. 8, solid lines). Here, whereas the situation remain similar for the fully hydrogenated $Si_{10}H_{16}$ cluster and for the $Si_{10}H_{14}{=}O$ cluster, in the case of the Si—O—Si bridge bond (Fig. 8(c)) an important excitonic peak, separated from the rest of the spectrum, is evident at ~1.5 eV. Actually bound excitons are present also in the fully hydrogenated (at 0.4 eV) and in the $Si_{10}H_{14}{=}O$ (at 1.0 eV) clusters, with calculated binding energies even larger than in the case of the Si—O—Si bridge bond (3.4 and 3.6 eV respectively, to be compared with a binding energy of 2.0 eV in the case of the bridge bond cluster). Nevertheless, the related transitions are almost dark and the emission intensity is very low. Only in the case of the Si—O—Si bridge bond the photoluminescence peak appears thanks to the strong oscillator strength of the related transition.

The bottom of Figure 8 shows the experimental absorption and emission spectra measured by Ma et al.[57] for Si-nanodots embedded in SiO_2 matrix. A strong photoluminescence peak appears around 1.5 eV. Comparison of the experimental spectra with our results suggests that the presence of a Si—O—Si bridge bond at the surface of Si-nc can explain the nature of luminescence in Si nanocrystallites: only in this case the presence of an excitonic peak in the emission related spectra, red shifted with respect to the absorption onset, provides an explanation for both the observed Stokes shift and the near-visible PL in Si-nc. It is worthwhile to stress that the role of the interface has been experimentally proven to be important for the PL properties of embedded Si-nc in SiO_2 (Ref. [58]) and in the mechanism of population inversion at the origin of the optical gain;[24, 58] besides, Monte Carlo approaches have demonstrated that Si—O—Si bridge bonds are the main building blocks in the formation of Si—SiO_2 flat interfaces[59] and form the low energy geometries at the interface for Si-nc embedded in silicon dioxide.[60] In conclusion, our theoretical results, obtained by ab-initio calculations and fully including excitonic effects, suggest that the Si—O—Si bridge bond is responsible for the strong PL peak experimentally observed, and shed some light on the role of the Si-nc—SiO_2 interface.

4. DOPING IN SI-NANOCRYSTALS

Another possibility for changing the optical properties of Si-nc is the use of doping. Actually it has been shown that the PL peak can be tuned also below the bulk Si band gap by properly controlling the impurities, for example by B and P co-doping.[30–32]

Theoretical studies of impurities in silicon quantum dots have lagged relative to calculations for pure, un-doped systems. Only few first principles studies are present in the literature, devoted to quantum confinement effects in single doped Si-nc.[61–63] The results point out that the ionization energy for the Si-nc is virtually size independent and that the donor and acceptor binding energies are substantially enhanced. Recently we have performed a preliminar theoretical study that considers also the simultaneous doping of Si-nc with *n*- and *p*-type impurities.[64] In this section we will present our recent results concerning the structural, electronic, and optical properties of single and co-doped silicon nanocrystals. The structural changes of the doped Si-nc have been investigated not only as a function of the size but also of the impurity position within the nanocluster and of the number of doping species. Our results have been obtained through a plane-wave, pseudopotential density functional calculation of impurity states in spherical Si-nc, with diameter ranging from 1.04 nm ($Si_{29}H_{36}$) to 2.24 nm ($Si_{293}H_{172}$). The Si-nc are built taking all the bulk Si atoms contained within a sphere of a given radius and terminating the surface dangling bonds with hydrogen. Each cluster is centered on a Si atom. We always consider, as in the experiments, B and P impurities in substitutional sites. Full relaxation with respect to the atomic positions is performed for both doped and un-doped systems. All the calculations have been performed using the ESPRESSO package,[53] within the GGA approximation using Vanderbilt ultrasoft[65] pseudopotentials. The Si-nc have been embedded in large supercells in order to prevent interactions between the periodic replicas (about 6 Å of vacuum separates neighbor clusters in all the considered systems). A careful analysis has been performed on the convergence of both the electronic and structural properties with respect to both the supercell side and plane-wave basis set cut-off. The structural and electronic properties, together with the impurity formation energy, are investigated as a function of the size and of the impurity position within the Si-nc. For the co-doped Si-nc the formation energies were compared with the corresponding single-doped cases. Indeed the absorption properties of the Si-nc have been calculated through the imaginary part of the dielectric function.

The first important point is related to the change of the structural properties induced by the impurity presence. It comes out that the amount of the relaxation around the impurity is directly related to the impurity valence. In particular a more significant distortion is found for the trivalent atoms (boron), for which one electron for the bonding with the surrounding Si atoms is missing. In fact, for the B-doped clusters, while the Si—Si bond lengths keep almost unchanged, some reconstruction occurs around the impurity. The overall structure has

C_{3v} symmetry, with an impurity displacement along the $\langle 111 \rangle$ direction when it is placed at the nanocluster center. Such displacement leads to one longer and three shorter (and equal) Si-impurity distances. While the longer bond is "almost" independent on the size, the shorter one decreases with the size. It is interesting to note that the relaxation of the bulk Si supercell containing the B impurity leads to an "almost" T_d configuration, in which the four B—Si bonds are practically the same. For pentavalent atoms, regarding the P-doped Si-nc, the relaxation leads to a nearly T_d symmetry,[61] in which the differences between the four P—Si bonds are negligible, less than 0.7%.

Starting from the Si_nH_m nanocluster,[33] the formation energy for the neutral X impurity can be defined as the energy needed to insert the X atom with chemical potential μ_X within the cluster after removing a Si atom (transferred to the external chemical reservoir, assumed to be bulk Si[61])

$$E_f = E(Si_{n-1}XH_m) - E(Si_nH_m) + \mu_{Si} - \mu_X$$

where E is the total energy of the system, μ_{Si} the total energy per atom of bulk Si, μ_X the total energy per atom of the impurity (We consider the total energy per atom in the tetragonal B_{50} crystal for B, and the orthorhombic black phosphorus for P). Our calculations clearly show that for smaller Si-nc a larger energy is needed for the formation of the impurity. For B-doped Si-nc a decreasing behavior of E_f versus $1/R$ is observed, that can be described by the linear formula

$$E_f = 0.80 + 4.64/R$$

where R is expressed in Å and E_f in eV, and the value $E_f = 0.80$ eV corresponds to doped bulk Si. For P-doped Si-nc the same decreasing behavior of E_f versus $1/R$ is observed, the linear formula is now

$$E_f = 0.21 + 4.98/R$$

The fact that the calculated formation energy is lower for larger Si-nc is in qualitative agreement with the observed suppression of the PL in doped Si nanocrystals. Fujii et al.[32] have shown that on increasing the annealing temperature both the Si-nc size increases and a stronger PL suppression is observed. This effect is a signature of an higher impurity concentration, thus showing that larger Si-nc can more easily sustain the doping.

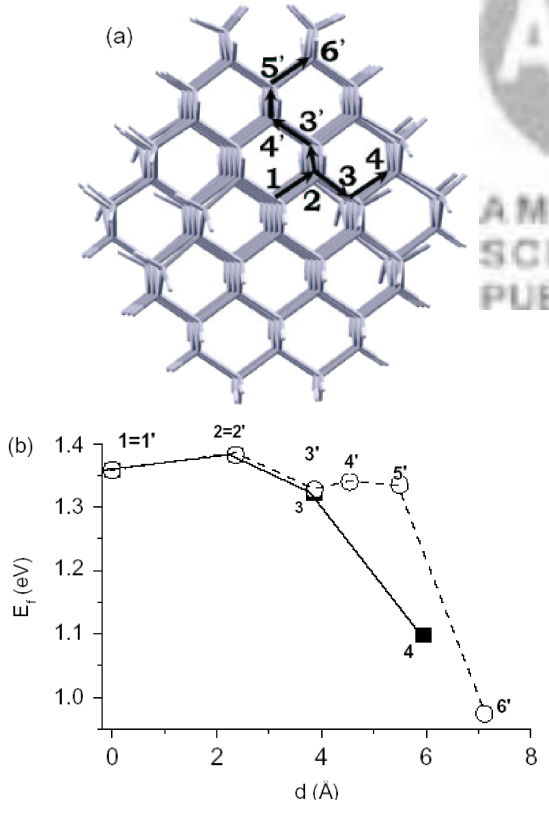

Fig. 9. Formation energies for neutral impurities as a function of the impurity position within the cluster (b). The impurity is moved along two different paths toward the surface, as shown in (a).

Table III. Bond lengths at the subsurface substitutional site where the impurities are located for the un-doped $Si_{87}H_{76}$ cluster and the single- and co-doped ones. Si_s and Si_i refer to surface and inner Si atoms around this site respectively.

Bond	$Si_{87}H_{76}$ Å	Bond	$Si_{86}BH_{76}$ Å	$Si_{86}PH_{76}$ Å	$Si_{85}BPH_{76}$ Å
Si—Si_s	2.355	B—Si_s	2.036		2.021
Si—Si_s	2.355	B—Si_s	2.036		2.021
Si—Si_i	2.363	B—Si_i	2.014		2.034
Si—Si_i	2.363	B—Si_i	2.014		2.034
Si—Si_s	2.355	P—Si_s		2.294	2.295
Si—Si_s	2.355	P—Si_s		2.294	2.295
Si—Si_i	2.363	P—Si_i		2.380	2.331
Si—Si_i	2.363	P—Si_i		2.380	2.331

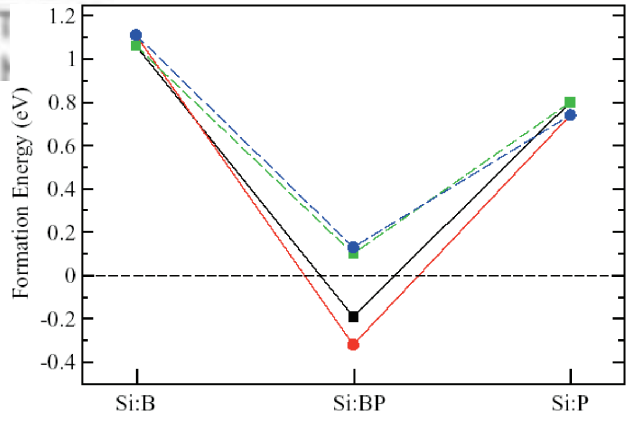

Fig. 10. Formation energy of the neutral impurities located at subsurface positions as a function of the doping: B (left) and P (right) single-doped and B-P (middle) co-doped nanoclusters are considered. The lines are a guide for the eyes. Dashed lines (green and blue): neutral impurities separated from each other by largest possible distances within the Si-nc, and solid lines (black and red): neutral impurities located at nearest neighbor distances in the co-doped clusters. Squares (green and black) are related to the $Si_{87}H_{76}$ nanoclusters, circles (red and blue) to the $Si_{147}H_{100}$ ones.

The formation energy changes also as a function of the impurity position within the Si-nc. When the impurity is moved from the cluster center toward the surface, an energy drop is found as the B impurity is moved to the Si layer just below the surface. In Figure 9 we show the formation energy for the B neutral impurity in the $Si_{146}BH_{100}$ cluster. The impurity is moved from the cluster center toward the surface along two paths, shown in Figure 9(a). The calculated energies are shown in Figure 9(b). On the x-axis we put the distance from the center of the replaced Si atom in the $Si_{147}H_{100}$ cluster. It comes out that as far as the replaced atoms moves within the internal core, variations not higher than 0.06 eV are found. Instead, a larger energy drop, of either 0.25 eV or 0.35 eV, is found as the B is moved to the Si layer just below the surface. This is explained by considering that such positions are the only which allow a significant reconstruction around the impurity, because in the other cases the surrounding Si cage is quite stable. Thus, as the B atom is moved toward the surface the formation energy decreases, making the positions underlying the surface more stable. Moreover in these cases the local structure has now a C_{2v} symmetry, with two shorter and two longer Si-impurity distances with respect to the surface and inner Si atoms (see Table III). Recently these findings have received an experimental support.[66]

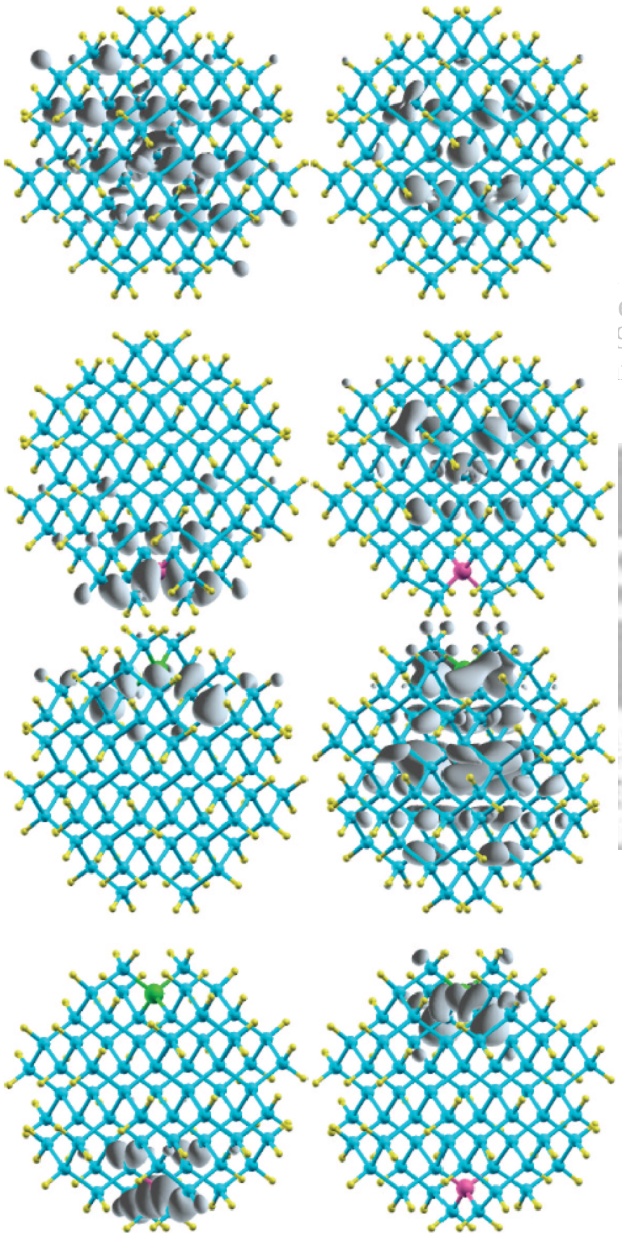

Fig. 11. From the top to the bottom: the HOMO (left) and LUMO (right) square modulus contour plots calculated for the $Si_{87}H_{76}$, the single-doped $Si_{86}BH_{76}$, the single-doped $Si_{86}PH_{76}$, and the co-doped $Si_{85}BPH_{76}$ nanoclusters. The isosurfaces correspond to 10% of the maximum value. B (violet) impurity is located at the bottom of the Si-nc, P (green) at the top. The Si atoms are cyan (gray) and the H atoms are yellow (light gray).

Table III gives the relaxed bond lengths around the impurity in subsurface positions for the $Si_{87}H_{76}$-nc (the results are quite similar for the $Si_{147}H_{100}$ ones). Both single- and co-doped cases have been considered. It is interesting to note that in the co-doped case the differences among the four impurity-Si bond lengths are clearly smaller with respect to the single-doped case. Thus, if carriers in the Si-nc are perfectly compensated by simultaneously doping with n- and p-type impurities, an almost T_d configuration is recovered in which the four impurity-Si bonds are practically the same.

This fact is reflected in the formation energy (FE) results. The FE's, are reported in Figure 10, for B-, P-doped, and B-P-co-doped Si-nc for two, different in size, Si-nc. In all cases the impurities are located in subsurface positions. The figure at the top is related to neutral impurities located at the largest possible distances, the bottom to impurities that are nearest neighbor. From Figure 10 it is clear that simultaneous doping strongly reduces (by about 1 eV) E_f with respect to both single-doped cases. This reduction is similar for Si-nc of different size. The important point here is that Si-nc can be more easily simultaneously doped than single-doped; this is a consequence of both the charge compensation and the minor structural deformation. Moreover the formation energy is lower when the impurities are nearest neighbor, thus confirming the important role played by electrostatic attraction.

Regarding the electronic properties the influence of single or co-doping is marked. The presence of donor or acceptor states lowers the HOMO-LUMO energy gap E_G of the un-doped Si-nc. For single-doped Si-nc the HOMO level now contains only one electron and is strongly localized either on B or P impurity. For example in the case of the $Si_{86}BH_{76}$ doped nanocrystals the defect level is located above the valence band and the energy gap is reduced from 2.59 to 2.31 eV, whereas for the $Si_{86}PH_{76}$ doped nanocrystals the defect level is located below the conduction band and the energy gap is now 0.28 eV. What is important is that the electronic properties of B- and P-co-doped

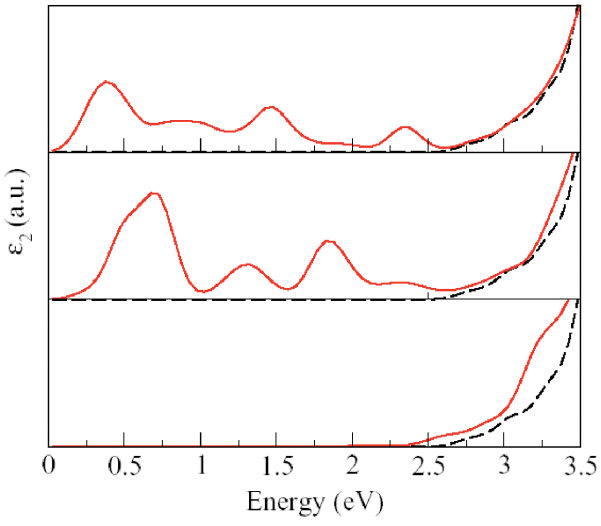

Fig. 12. Top panel: DFT-LDA calculated imaginary part of the dielectric function (ε_2) for the $Si_{86}BH_{76}$ single-doped cluster, red. Center panel: the same for the $Si_{86}PH_{76}$ single-doped cluster. Bottom panel: the same for the $Si_{85}BPH_{76}$ co-doped cluster. In all panels the result for the ε_2 of the un-doped $Si_{87}H_{76}$ cluster (dashed line, black) is reported for comparison. A Gaussian broadening of 0.1 has been used.

Si-nc are qualitatively and quantitatively different from those of either B- or P-doped Si-nc. For the $Si_{85}BPH_{76}$ nanocrystals E_G is lowered from 2.59 eV (pure Si-nc) to 1.82 eV (co-doped Si-nc). The results for the $Si_{145}H_{100}$ case are similar: E_G reduces from 2.30 eV of the pure Si-nc to 1.56 eV of the $Si_{145}BPH_{100}$ nanocrystal. For pure Si-nc larger than those considered here, having a smaller E_G, it would be possible by co-doping to obtain an E_G even smaller than the bulk Si bandgap in agreement with the experimental outcomes.[30, 32] Besides on going from the pure, to the single-, to the co-doped Si-nc the HOMO and LUMO states progressively localize on the impurities. In the co-doped case the HOMO is strongly localized on the B impurity and the LUMO on the P impurity (see Fig. 11 that visualizes the calculated square modulus contour plots related to HOMO and LUMO states, showing their localization within the Si-nc).

These facts have a profound influence on the optical properties of the Si-nc. The optical properties have been calculated through the imaginary part ε_2 of the dielectric function. Due to the strong confinement effects, only transitions at the Γ point have been considered. Figure 12 reports our calculated imaginary parts of the dielectric function (ε_2) for the $Si_{87}H_{76}$ clusters. We consider B- (top panel), P- (center panel) single doped nanocrystals, and the B and P co-doped (bottom panel) nanocrystal. In all cases the result is compared with the corresponding one for the un-doped $Si_{87}H_{76}$ clusters. Concerning the un-doped cases we see that several new peaks appear in the low energy region between 0 and 2 eV. These peaks are due to the "interband" and "intraband" transitions that involve the impurity state, that is located in the band energy gap. These new features could be important for applications in the infrared region and in Raman lasers technology. For the co-doped $Si_{85}BPH_{76}$ cluster, as shown at the bottom of Figure 12, we note the shift of the optical gap to lower energies and the rise of new strong features not present for the un-doped $Si_{87}H_{76}$ cluster. The enhancement of the intensity in this region is a direct consequence of the localization process of the HOMO and LUMO states on the impurities described above. One can expect for the exciton an enhancement of the intensity as consequence of the localization process. This is confirmed by the results for the HOMO and LUMO localization for the same co-doped $Si_{85}BPH_{76}$ cluster when the B and P impurities are nearest

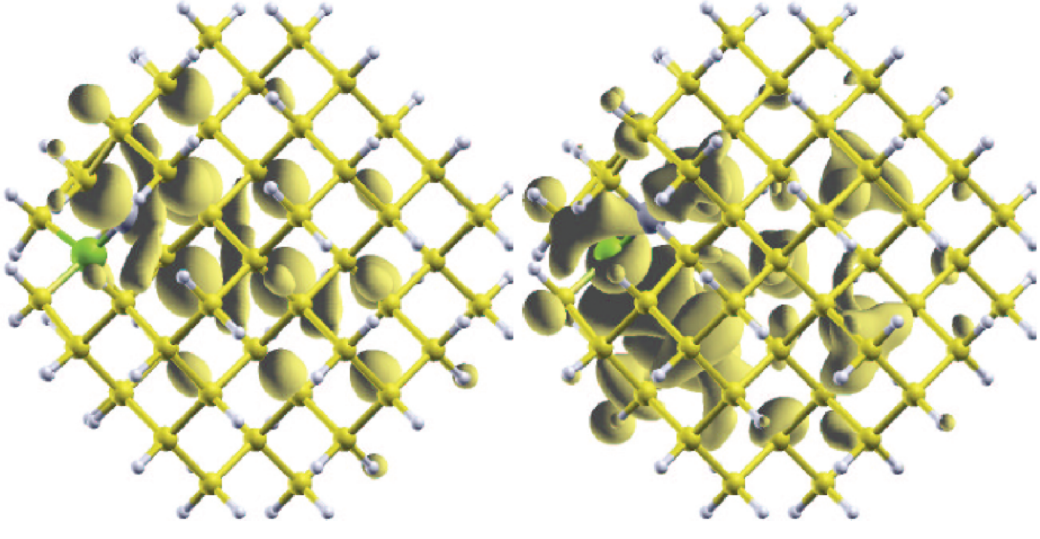

Fig. 13. The HOMO (left) and LUMO (right) square modulus contour plots calculated for the co-doped $Si_{85}BPH_{76}$ nanoclusters with B (gray) and P (green) impurities as first nearest neighbor. The Si atoms are yellow, and the H atoms are white. The isosurfaces correspond to 10% of the maximum value.

neighbor, that show an increase in the overlap between the two states (see Fig. 13).

These outcomes can explain the experimental data,[30, 32] which show a PL intensity for co-doped Si-nc even higher than that of pure Si-nc and have demonstrated that by co-doping it is possible to shift the PL peak even below the Si bulk band gap.

5. CONCLUSIONS

In this paper we have presented the results of first-principle calculations related to the structural, electronic, and optical properties of semiconductor nanostructures. In our investigations we considered both un-doped and doped Si-based nanocrystals, with diameters ranging up to 2.5 nm. Particular attention has been paid to the outcomes related to the nanocrystals excited state. In particular we have found that:

(i) the presence of an electron-hole pair in the nanocrystals causes a strong deformation of the structures with respect to their ground-state configuration, and this is more evident for the smaller systems,

(ii) a significant contribution to the Stokes shift arises from structural relaxation after excitation of the nanocluster, thus considering the HOMO-LUMO gaps of the ground and excited state as the proper absorption and emission energies is worse predicted the smaller is the cluster,

(iii) concerning the absorption spectra, the inclusion of many-body effects within BSE or TDLDA gives results that are quite similar regarding the absorption onset and in agreement with the experimental outcomes,

(iv) the oxidation of the Si-nc induces structural modification and significant changes in the electronic properties that depend on the type of the Si—O bond,

(v) the full inclusion of the excitonic effects in the calculation of the emission spectra suggest that the Si—O—Si bridge bond is responsible for the strong PL peak experimentally observed in oxidized Si-nc,

(vi) the Si-nc can be more easily simultaneously doped than single-doped,

(vii) finally, by co-doping it is possible to engineer the PL properties of the Si-nc.

Acknowledgments: This work has been done within the CNISM Project. We acknowledge also the support of the MIUR COFIN-PRIN (2005) Italy. All the calculations were performed at CINECA-Bologna ("Iniziativa Calcolo Parallelo-CNR-INFM"), CICAIA-Modena, and Campus Computational Grid-Napoli advanced computing facilities.

References and Notes

1. S. Ossicini, L. Pavesi, and F. Priolo, Light emitting silicon for microphotonics, Springer Tracts on Modern Physics, Springer-Verlag, Berlin **(2003)**, Vol. 194.
2. L. Pavesi and E. Buzaneva, Frontiers of Nano-optoelectronics systems, NATO Science Series II. Mathematics, Physics and Chemistry, Kluwer Academic Publishers, Dordrecht **(2000)**, Vol. 6.
3. L. T. Canham, *Appl. Phys. Lett.* 57, 1046 **(1990)**.
4. D. Bensahel, L. T. Canham, and S. Ossicini (Eds.), Optical Properties of Low Dimensional Silicon Structures, Kluwer, Dordrecht, Amsterdam **(1993)**.
5. B. Hamilton, *Semicond. Sci. Technol.* 10, 1187 **(1995)**.
6. Y. Kanemitsu, *Phys. Rep.* 263, 1 **(1995)**.
7. G. S. John and V. A. Singh, *Phys. Rep.* 263, 93 **(1995)**.
8. L. T. Canham (Ed.), Properties of Porous Silicon, INSPEC: The Institution of Electrical Engineers, London **(1997)**.
9. A. G. Cullis, L. T. Canham, and P. D. J. Calcott, *J. Appl. Phys.* 82, 909 **(1997)**.
10. O. Bisi, S. Ossicini, and L. Pavesi, *Surf. Sci. Reports* 38, 5 **(2000)**.
11. Y. Takahashi, T. Furuta, Y. Ono, T. Tsishima, and M. Tabe, *Jpn. J. Appl. Phys.* 34, 950 **(1995)**.
12. D. J. Lockwood, Z. H. Lu, and J.-M. Baribeau, *Phys. Rev. Lett.* 76, 539 **(1996)**.
13. S. V. Novikov, J. Sinkkonen, O. Kilpela, and S. V. Gastev, *J. Vac. Sci. Technol. B* 15, 1471 **(1997)**.
14. Y. Kanemitsu and S. Okamoto, *Phys. Rev. B* 56, R15561 **(1997)**.
15. V. Mulloni, R. Chierchia, C. Mazzoleni, G. Pucker, L. Pavesi, and P. Bellutti, *Phil. Mag. B* 80, 705 **(2000)**.
16. R. J. Baierle, M. J. Caldas, E. Molinari, and S. Ossicini, *Solid State Commun.* 102, 545 **(1997)**.
17. M. V. Wolkin, J. Jorne, P. M. Fauchet, G. Allan, and C. Delerue, *Phys. Rev. Lett.* 82, 197 **(1999)**.
18. A. Puzder, A. J. Williamson, J. C. Grossman, and G. Galli, *Phys. Rev. Lett.* 88, 097401 **(2002)**.
19. M. Luppi and S. Ossicini, *Phys. Rev. B* 71, 035040 **(2005)**.
20. M. Luppi and S. Ossicini, *Phys. Stat. Sol. (a)* 197, 251 **(2003)**.
21. M. Luppi and S. Ossicini, *J. Appl. Phys.* 94, 2130 **(2003)**.
22. I. Vasiliev, J. R. Chelikowsky, and R. M. Martin, *Phys. Rev. B* 65, 121302(R) **(2002)**.
23. L. Pavesi, L. Dal Negro, C. Mazzoleni, G. Franzò, and F. Priolo, *Nature* 408, 440 **(2000)**.
24. L. Dal Negro, M. Cazzanelli, L. Pavesi, S. Ossicini, D. Pacifici, G. Franzò, F. Priolo, and F. Iacona, *Appl. Phys. Lett.* 82, 4636 **(2003)**.
25. J. Ruan, P. M. Fauchet, L. Dal Negro, M. Cazzanelli, and L. Pavesi, *Appl. Phys. Lett.* 83, 5479 **(2003)**.
26. M. Cazzanelli, D. Kovalev, L. Dal Negro, Z. Gaburro, and L. Pavesi, *Phys. Rev. Lett.* 93, 207042 **(2004)**.
27. S. Ossicini, C. Arcangeli, O. Bisi, E. Degoli, M. Luppi, R. Magri, L. Dal Negro, and L. Pavesi, Towards the first silicon laser, Nato Science Series, edited by L. Dal Negro, S. Gaponenko, and L. Pavesi, Kluwer Academic Publishers, Dordrecht **(2003)**, Vol. 93, p. 271.
28. G. Allan, C. Delerue, and M. Lannoo, *Phys. Rev. Lett.* 76, 2961 **(1996)**.
29. C. Delerue, G. Allan, and M. Lannoo, *J. Lum.* 80, 65 **(1999)**.
30. M. Fujii, Y. Yamaguchi, Y. Takase, K. Ninomiya, and S. Hayashi, *Appl. Phys. Lett.* 87, 211919 **(2005)**.
31. M. Fujii, K. Toshikiyo, Y. Takase, Y. Yamaguchi, and S. Hayashi, *J. Appl. Phys.* 94, 1990 **(2003)**.
32. M. Fujii, Y. Yamaguchi, Y. Takase, K. Ninomiya, and S. Hayashi, *Appl. Phys. Lett.* 85, 1158 **(2004)**.
33. E. Degoli, G. Cantele, E. Luppi, R. Magri, D. Ninno, O. Bisi, and S. Ossicini, *Phys. Rev. B* 69, 155411 **(2004)**.
34. X. Gonze, J.-M. Beuken, R. Caracas, F. Detraux, M. Fuchs, G.-M. Rignanese, L. Sindic, M. Verstraete, G. Zerah, F. Jollet, M. Torrent, A. Roy, M. Mikami, Ph. Ghosez, J.-Y. Raty, and D. C. Allan, *Comp. Mat. Science* 25, 478 **(2002)**.
35. A. Franceschetti and S. T. Pantelides, *Phys. Rev. B* 68, 033313 **(2003)**.
36. R. W. Godby and I. D. White, *Phys. Rev. Lett.* 80, 3161 **(1998)**; A. Franceschetti, L. W. Wang, and A. Zunger, *Phys. Rev. Lett.* 83, 1269 **(1999)**.

37. H.-C. Weissker, J. Furthmüller, F. Bechstedt, *Phys. Rev. Lett.* 90, 085501 **(2003)**.
38. A. Puzder, A. J. Williamson, J. C. Grossman, and G. Galli, *J. Am. Chem. Soc.* 125, 2786 **(2003)**.
39. H.-C. Weissker, J. Furthmüller, and F. Bechstedt, *Phys. Rev. B* 67, 245304 **(2003)**.
40. L. Pizzagalli, G. Galli, J. E. Klepeis, and F. Gygi, *Phys. Rev. B* 63, 165324 **(2001)**.
41. C. Delerue, M. Lannoo, and G. Allan, *Phys. Rev. Lett.* 84, 2457 **(2000)**.
42. J. C. Grossman, M. Rohlfing, L. Mitas, S. G. Louie, and M. L. Cohen, *Phys. Rev. Lett.* 86, 472 **(2001)**.
43. G. Onida and W. Andreoni, *Chem. Phys. Lett.* 243, 183 **(1995)**.
44. The absorption gap value for the $Si_{29}H_{36}$ cluster cited by Franceschetti is 4.3 eV but it is estimated by adding the local-spin density band-gap error of bulk Si (0.7 eV).
45. U. Itoh, Y. Toyoshima, H. Onuki, N. Washida, and T. Ibuki, *J. Chem. Phys.* 85, 4867 **(1986)**.
46. M. Hirao, Microcrystalline and Nanocrystalline Semiconductors, edited by L. Brus, M. Hirose, R. W. Collins, F. Koch, and C. C. Tsai, *Mater. Res. Soc. Symp. Proc.*, No. 358, Material Research Society, Pittsburgh **(1995)**, p. 3.
47. O. Lehtonen and D. Sundholm, *Phys. Rev. B* 72, 085424 **(2005)**.
48. G. Belomoin, J. Therrien, A. Smith, S. Rao, R. Twesten, S. Chaieb, M. H. Nayfeh, L. Wagner, and L. Mitas, *Appl. Phys. Lett.* 80, 841 **(2002)**.
49. Y. Kanemitsu and S. Okamoto, *Phys. Rev. B* 58, 9652 **(1998)**.
50. M. Gatti and G. Onida, *Phys. Rev. B* 72, 045442 **(2005)**.
51. A. B. Filonov, S. Ossicini, F. Bassani, and F. Arnaud D'Avitaya, *Phys. Rev. B* 65, 195317 **(2002)**.
52. E. Luppi, E. Degoli, G. Cantele, S. Ossicini, R. Magri, D. Ninno, O. Bisi, O. Pulci, G. Onida, M. Gatti, A. Incze, and R. Del Sole, *Opt. Mater.* 27, 1008 **(2005)**.
53. S. Baroni, A. Dal Corso, S. de Gironcoli, P. Giannozzi, C. Cavazzoni, G. Ballabio, S. Scandolo, G. Chiarotti, P. Focher, A. Pasquarello, K. Laasonen, A. Trave, R. Car, N. Marzari, and A. Kokalj, The DFT calculations have been performed using the ESPRESSO package. http://www.pwscf.org/.
54. L. Hedin, *Phys. Rev.* 139, A796 **(1965)**.
55. G. Onida, L. Reining, and A. Rubio, *Rev. Mod. Phys.* 74, 601 **(2002)** and references therein.
56. F. Bassani and G. Pastori Parravicini, Electronic States and Optical Transitions in Solids, Pergamon Press, New York **(1975)**.
57. Z. Ma, X. Liao, and G. Kong, *J. Chu, Appl. Phys. Lett.* 75, 1857 **(1999)**.
58. N. Daldosso, M. Luppi, S. Ossicini, E. Degoli, R. Magri, G. Dalba, P. Fornasini, R. Grisenti, F. Rocca, L. Pavesi, S. Boninelli, F. Priolo, C. Spinella, and F. Iacona, *Phys. Rev. B* 68, 085327 **(2003)**.
59. Y. Tu and J. Tersoff, *Phys. Rev. Lett.* 89, 086102 **(2002)**.
60. G. Hadjisavvas and P. Kelires, *Phys. Rev. Lett.* 93, 226104 **(2004)**.
61. D. V. Melnikov and J. R. Chelikowsky, *Phys. Rev. Lett.* 92, 046802 **(2004)**.
62. G. Cantele, E. Degoli, E. Luppi, R. Magri, D. Ninno, G. Iadonisi, and S. Ossicini, *Phys. Rev. B* 72, 113303 **(2005)**.
63. Z. Zhou, M. L. Steigerwald, R. A. Friesner, L. Brus, and M. S. Hybertsen, *Phys. Rev. B* 71, 245308 **(2005)**.
64. S. Ossicini, E. Degoli, F. Iori, E. Luppi, R. Magri, G. Cantele, F. Trani, and D. Ninno, *Appl. Phys. Lett.* 87, 173120 **(2005)**.
65. D. Vanderbilt, *Phys. Rev. B* 41, R7892 **(1990)**.
66. E. Garrone, F. Geobaldo, P. Rivolo, G. Amato, L. Boarino, M. Chiesa, E. Giamello, R. Gobetto, P. Ugliengo, and A. Vitale, *Adv. Mat.* 17, 528 **(2005)**.

Received: 23 June 2006. Revised/Accepted: 18 January 2007.